Conduction-band structure of graphite studied by combined angle-resolved inverse photoemission and target current spectroscopy

I. Schäfer, M. Schlüter, and M. Skibowski
Institut für Experimentalphysik, Universität Kiel, 2300 Kiel 1, Federal Republic of Germany
(Received 15 December 1986)

The dispersion of the conduction states parallel to the basal plane of highly oriented pyrolitic graphite was investigated up to 28 eV above the Fermi level by inverse photoemission with the use of a new highly efficient band-pass photon detector. The remarkable modulation of the absorbed target current as a function of the kinetic energy of the incident electrons is interpreted as an elastic reflection phenomenon. As in inverse photoemission, the current spectra show a strong dependence on the angle of incidence and provide additional information about the conduction-band structure from the vacuum level up to 38 eV above the Fermi level. The results of both methods are compared with recent band-structure calculations. Besides several π and σ bands, an image-potential state is observed just below the lowest σ band. The extraordinary width of this σ band along the c axis was directly examined by current spectroscopy.

I. INTRODUCTION

Graphite as the prototype of layered structures and its variety of intercalation compounds have attracted considerable attention both theoretically and experimentally during the last decades. Numerous band-structure calculations[1–5] exhibit in general a similar shape of the electronic structure. The valence-band σ states derived from $2s$, $2p_x$, $2p_y$ atomic orbitals (sp^2 hybrides) form strong covalent intralayer bonding and extend to higher binding energies than the $2p_z$-derived π states. The full band structure consists of bonding π, σ states and antibonding π^*, σ^* states which build the valence and conduction bands, respectively. In the direct vicinity of the Fermi level there exist only π and π^* states. The entire band structure is characterized by a pronounced paraboliclike dispersion parallel to the surface and (not regarding a few bands with mainly p_z character) by a strong localization perpendicular to the basal plane. Thus graphite can be considered as a model substance of a two-dimensional solid. Recent band-structure calculations[1–3,6,7] going beyond the tight-binding approximation with a basis of only $2s$, $2p$ orbitals of carbon found a σ state as the lowest conduction band at Γ which has, in deviation from the simple picture of nearly two-dimensionality, a large dispersion perpendicular to the surface with considerable charge density between the layers (interlayer state).

The dispersion and binding energy of the occupied states has recently been well established by angle-resolved photoelectron spectroscopy[8–14] (ARPES) in reasonable agreement with the calculations. On the other hand, little experimental data for the unoccupied part of the band structure is available and most results are concerned only with the density of states. The calculations differ significantly as regards energy location and dispersion in this region of the electronic structure. The only wave-vector-resolved data available on unoccupied states is deduced from angle-resolved secondary electron spectroscopy (ARSEES) (Refs. 10, 15, and 16) above the vacuum level and angle-resolved inverse photoemission (ARIPS) (Refs. 17–20) down to the Fermi level.

Here we present the first detailed mapping of the unoccupied band structure obtained on highly oriented pyrolytic graphite (HOPG) for the wave vector parallel to the surface ($k_{||}$) by ARIPS (up to 23 eV above the Fermi level E_F), combined with angle-resolved target-current spectroscopy (TCS) (up to 38 eV above E_F) providing supplemental direct information about the unoccupied states.[18] The data are used to test recent theoretical results.

II. ANGLE-RESOLVED INVERSE PHOTOEMISSION SPECTROSCOPY AND TARGET-CURRENT SPECTROSCOPY EXPERIMENTAL SETUP

ARIPS is a rapidly developing method[21-23] for wave-vector-resolved investigations of unoccupied states, quite similar to ARPES in its theoretical foundation.[24] In ARIPS the intensity of the vacuum ultraviolet radiation (bremsstrahlung) generated by low-energy electrons impinging on the sample is measured. The radiation resulting from direct transitions between the initial LEED states and final states above the Fermi level shows strong intensity variation with angle of electron incidence containing information about the wave vector conserved in the transitions. From the photon energy, the kinetic energy $E_{\rm kin}$ and the polar angle ϑ of the incoming electron a two-dimensional experimental band structure $E(k_{||})$ can be deduced similar to the procedure in ARPES.

In TCS simply the current absorbed by the sample is measured as a function of $E_{\rm kin}$ of the electrons impinging on the sample under a defined angle. The absorbed (target) current I_T may be written as $I_T = I_0(1-R_e-R_i)$. Here $I_0(E_{\rm kin})$ is the incoming electron current, $R_e(E_{\rm kin})$ is the elastic and $R_i(E_{\rm kin})$ the inelastic electron reflectivity. $R_e(E_{\rm kin})$ describes the normalized flux of all outgoing LEED beams. In the following we attribute the modulation of the absorbed current exclusively to an elastic scattering phenomenon.[25–27] R_i is assumed to be an only

slowly varying function of energy not responsible for the modulation. R_i and I_0 only produce a smooth background. This interpretation differs from other work in which inelastic processes are considered to explain the modulation in the TCS spectra.[28,29] With the above assumptions the modulation in TCS apparently corresponds to an angle integrated LEED experiment. Due to the close relationship between the LEED reflectivity and the band structure very useful information about the unoccupied states above the vacuum level E_{vac} is directly deductable from the current modulation.[26,27] High reflectivity corresponding to a minimum in the target current I_T is expected, if the electron energy falls into a gap of the band structure projected onto the surface or if the symmetry of the wave function of the states in the solid does not allow matching of the incoming plane wave at the surface. On the other hand, regions of enhanced target current are expected at energies where the incoming electrons couple effectively to Bloch states of the crystal.

The components of the ARIPS spectrometer[30] are a band-pass photon detector ($\hbar\omega = 9.8$ eV) and an electron source optimized for low energies. The band-pass system consists of an open, focused mesh CuBe multiplier with KBr-coated first dynode (photocathode) and a CaF_2 entrance window, defining the high- and low-pass filters, respectively. Its efficiency[31] is about 1 order of magnitude higher than for the commonly used I_2-He-filled Geiger-Müller counter. The wave-vector resolution of the electron gun is 0.08 Å^{-1} and its energy resolution 220 meV (FWHM). The overall energy resolution of the ARIPS spectrometer is ~ 600 meV. The same electron gun is used in both ARIPS and TCS.

The TCS spectra presented in Sec. III are not normalized with respect to the incoming beam current which is only a slowly increasing function of energy not affecting the interpretation of the spectra. Except for one measurement with a slightly negative biased sample (~ -4.5 V) (Fig. 5) used to check the vicinity of the vacuum level, all TCS data were obtained under field-free conditions at the sample to avoid distortions of the electron beam which would deteriorate the angular resolution. To resolve weaker features the negative second derivative of the spectra obtained by careful filtering and differentiation has been used.

The sample of pyrolytic graphite (HOPG, Union Carbide) was cleaved in ultrahigh vacuum. No significant azimuthal dependence of the spectra was observed due to the rotational disorder of the HOPG. Standard $k_{||}$ analysis yields the two-dimensional experimental band structure fully compiled in Figs. 7 and 8.

III. RESULTS AND DISCUSSION

A. Inverse photoemission

Figures 1, 2, and 3 show the ARIPS spectra obtained for different ranges of energy and angle of electron incidence. The observed bands and their dispersions are labeled by capital letters A–I together with tick marks. The most intense *emission A* in the ARIPS spectra (Fig. 1) is the strong band which disperses to higher energies for decreasing angle of incidence. Simultaneously it drastically loses intensity and vanishes at about 20°. Its dispersion is in excellent agreement with the antibonding $\pi(M_3^+, {}_4^-)$ bands of the calculation of Holzwarth *et al.*[1] At an angle around 77° which is very close to the $k_{||}$ value corresponding to the $M(L)$ point a nondispersive localized *shoulder B* at about 1.5 eV above E_F merges with this π band. A similar step like nondispersive emission with a binding energy of 3 eV is visible in ARPES spectra.[9,10] It has been suggested that the shoulder in the ARPES measurements results from a surface state or emission out of isolated carbon atoms sitting on top of the outermost atomic plane.[9] But the shoulders for both states, occupied and unoccupied, lie within the experimental error at the energies of the bonding and antibonding π bands at $M(L)$ where those bands have their highest density of state (DOS). Thus the appearance of the localized shoulder can be considered as a contribution of non-$k_{||}$-conserving

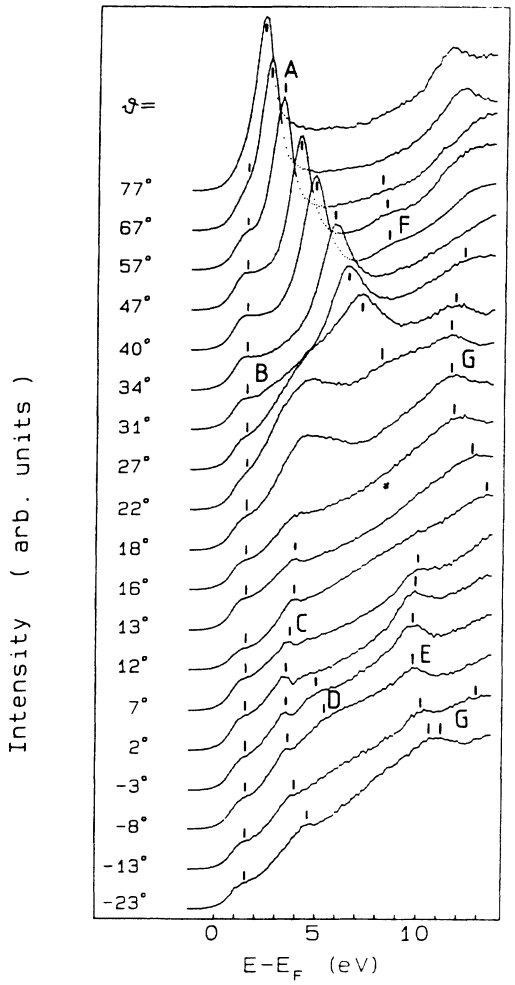

FIG. 1. Inverse photoemission spectra ($\hbar\omega = 9.8$ eV) up to 13 eV above the Fermi level E_F for various angles of electron incidence ϑ. The dispersion of the states labeled A–G is marked by ticks.

emission associated with a high DOS, probably caused by phonon or defect scattering of the LEED states involved in ARPES and ARIPS. The energy difference between the occupied and unoccupied shoulder (4.5—4.7 eV) is in good agreement with the measured critical transition of 4.5 eV (Ref. 32) and the calculated $M_3^+ - M_4^-$ separation varying from 4.1 (Ref. 3) to 4.8 eV (Ref. 4).

The *emission C* at 3.7 eV (for $k_{\|}=0$) has been studied in detail (Fig. 2). It is a parabolically dispersing peak with a FWHM and shape corresponding to the spectrometer function of the ARIPS system. In a photon-energy-dependent ARIPS measurement it was found to be a state without $k_{\perp}$ dispersion.[17] It is also the only state on graphite which significantly loses intensity by surface contamination.[33] Thus it is clearly a surface state. In slab calculations this state has been interpreted as split off the lowest $\sigma(\Gamma_1^+)$ band, the interlayer state.[7] But we suggest it is simply connected with the $n=1$ image potential state[21] existing in the gap below the interlayer band. The calculated binding energy of the surface state of nearly $\frac{1}{16}$ Ry ($k_{\|}=0$) with respect to the vacuum level[7] and the charge density of the state (free-electron-like parallel to the surface with a maximum at about 2 Å in front of the outermost carbon plane obtained in the slab calculation) is consistent with this interpretation. The experimental binding energy with respect to the independently determined E_{vac} (by TCS, see Sec. III B) is 1.0 eV and the effective band mass derived from the measured dispersion is

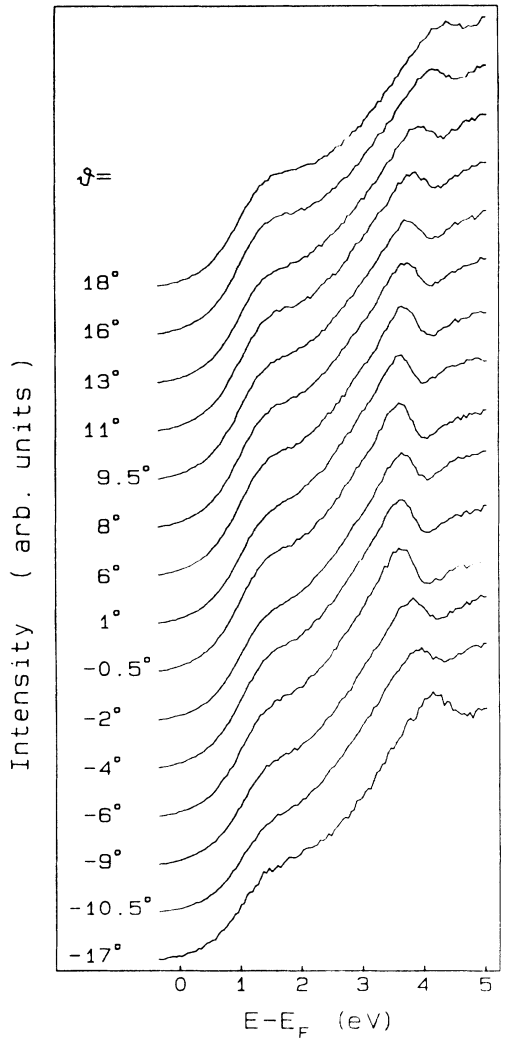

FIG. 2. Inverse photoemission spectra in the region of the ($n=1$) image potential (surface) state. The vacuum level ($E_{\text{vac}}-E_F$) is at 4.7 eV.

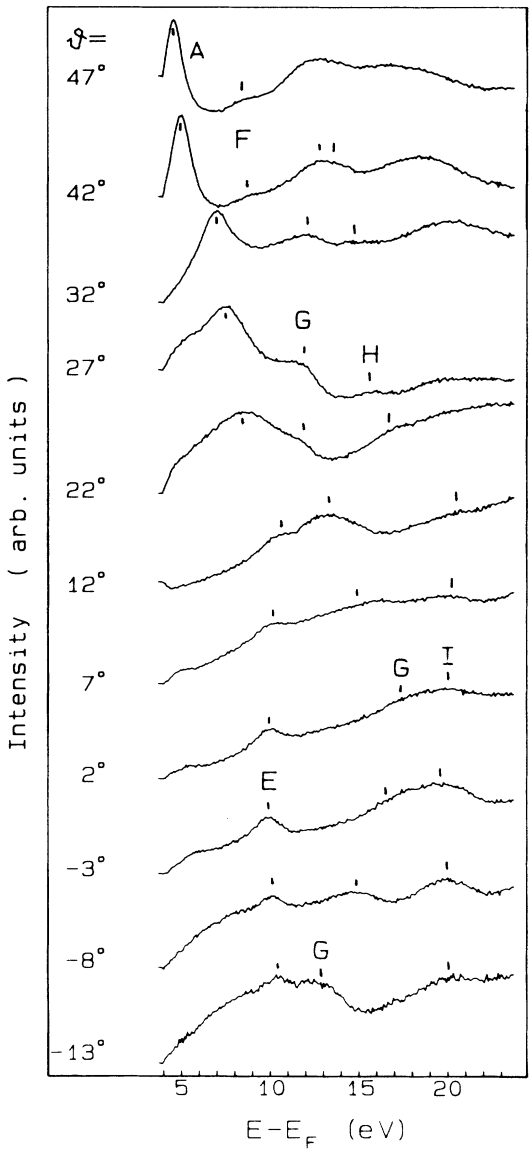

FIG. 3. Some inverse photoemission spectra taken at higher energies. The dispersion of the states labeled $A-I$ is marked by ticks.

$1.3m_0$. The weak shoulder just above the $n=1$ state is interpreted as emission due to higher members of the Rydberg series (clearly visible in Fig. 6). In Ref. 20, where a normal incidence inverse photoemission spectrum has recently been published, the state C is interpreted as density of state emission connected with the bottom of the interlayer state as already suggested by Fauster *et al.*[17] But the $k_{||}$ dispersion measured in our work clearly excludes this interpretation as a DOS effect. The amount of exposure to activated O_2 (33 L) and H_2 (150 L) to test the surface-state character of the emission in Ref. 20 seems far too low to affect an image potential state on an inert surface like that of graphite. But we agree with Reihl *et al.*[20] that a volume-induced surface state as a state split off the interlayer state should have been quenched already by small exposures to activated gases. We believe the $\sigma(\Gamma_1^+)$ band above the surface state becomes only visible as faint *emission (D)* at $-8°$, $-3°$ around 5 eV (Fig. 1). This is explainable by the low cross section of transitions to s-like bands which is much smaller than for p states at the photon energy involved (9.8 eV).

The *emission E* at 9.7 eV ($k_{||}=0$) is attributed to the $\sigma(\Gamma_5^+,_6^-)$ state in good agreement with the calculation of Holzwarth *et al.*[1] and the ARIPS measurement for normal incidence of Ref. 17. For increasing angles of incidence its intensity decreases and finally vanishes. This may be caused by the azimuthal disorder of the sample, since the dispersions of the four bands emerging from the two states at Γ are different in the ΓALM and ΓAHK plane.

One has to note that the energy location of this antibonding $p_{x,y}$-derived $\sigma(\Gamma_5^+,_6^-)$ band is controversial, because there is a large secondary electron maximum at 3 eV kinetic energy corresponding to 7.7 eV above the Fermi level which has been attributed to this state[10,15,16] in agreement with the calculation of Tatar and Rabii.[2] But neither is there emission at this energy in this ARIPS measurement or in the data of Fauster *et al.*[17] which cover a large range of the photon energy, nor is there any structure in the TCS data, although TCS and ARSEES have a similar theoretical foundation. Finally measurements of the unoccupied density of states obtained by different methods[34–36] reveal the first maximum of the antibonding σ states at about 8.5 eV in agreement with the measured energy of the σ states at M in this work. These $\sigma(M_1^+,_2^-)$ bands at $M(L)$ are visible as a weak dispersing *emission F*. Here the azimuthal disorder is probably overcome by the high DOS in the flat part of these bands near

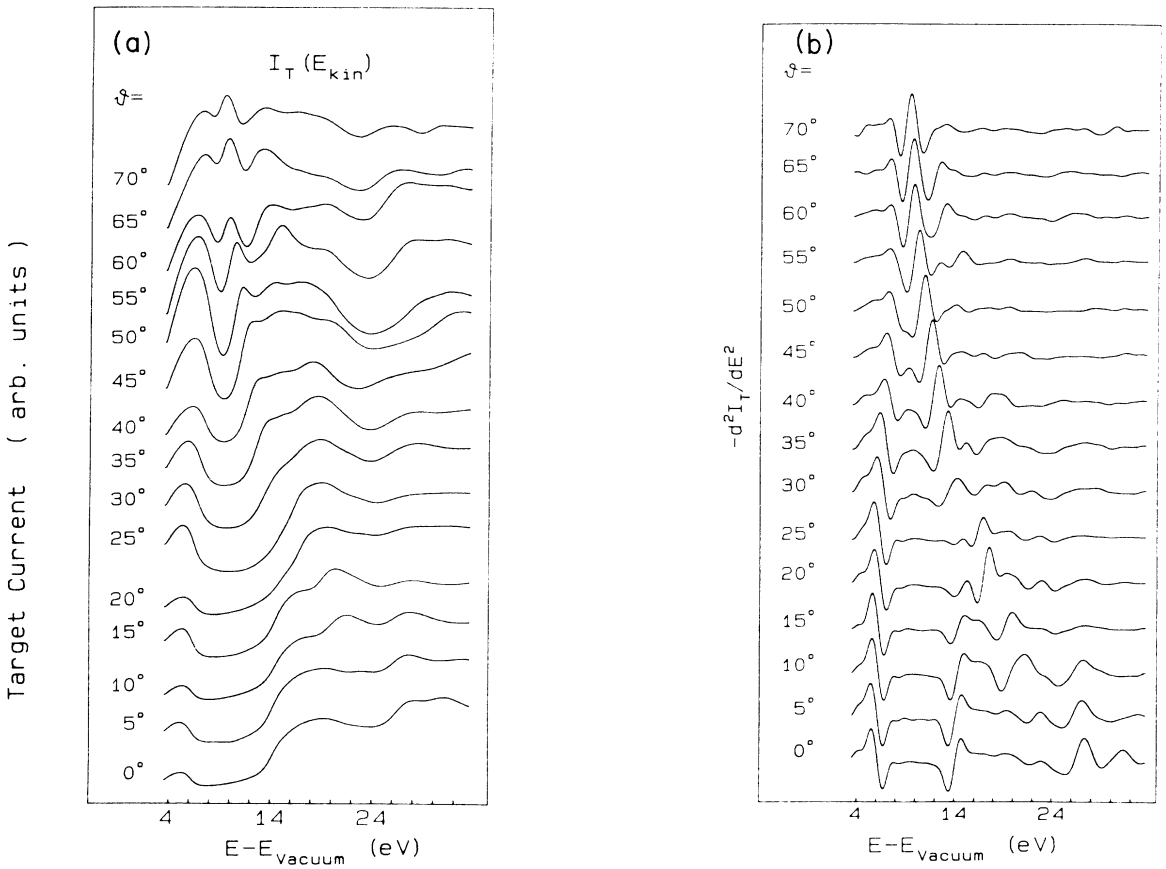

FIG. 4. The current I_T absorbed by the sample for various angles of electron incidence ϑ as a function of the kinetic energy (a). The negative second derivative of the current spectra (b).

the $M(L)$ point. So we believe that the interpretation of this strong secondary maximum as a conduction state is not correct and its origin is not understood yet.

The relatively intense and strongly dispersing *emission G* between 12 and 17 eV in Figs. 1 and 3 is somewhat puzzling because there is no such band in the two calculations in this higher-energy range.[2,5] But other calculations[1,3] show small portions of π bands attributable to this emission. The weak *structure H* around 42° probably corresponds to the strongly dispersing $\pi(\Gamma_2^-, M_3^+, K_6)$ band extending from 13 eV (at K) to 26 eV (at Γ) in the calculations of Tatar and Rabii[2] (Fig. 8). The *band I* at 20 eV is attributable to the $\sigma(\Gamma_4^-)$ band.[2] This band and the π band are also observed in TCS and ARSEES (Ref. 13) and will be discussed below in more detail.

B. Target current spectroscopy

Let us now turn to the discussion of the TCS data presented in Figs. 4–6 and compare the TCS results with those of inverse photoemission. Graphite shows a remarkable current modulation. This is to our knowledge the strongest modulation ever observed. For layered transition-metal dichalcogenides we have measured a somewhat weaker modulation. In three-dimensional materials like III-V compounds the modulation is 1 order of magnitude smaller but still significantly larger than for Cu. The stronger modulation for layered materials is probably explainable by many large gaps in the surface-projected band structure resulting from the smaller $k_\perp$ dispersion in more two-dimensional materials.

Figure 4 shows the original TCS spectra and their negative second derivative with the angle of electron incidence as parameter. Considerable structure is observed in the TCS spectra. It is related to the conduction-band states and their dispersion (cf. Sec. II). Especially interesting is

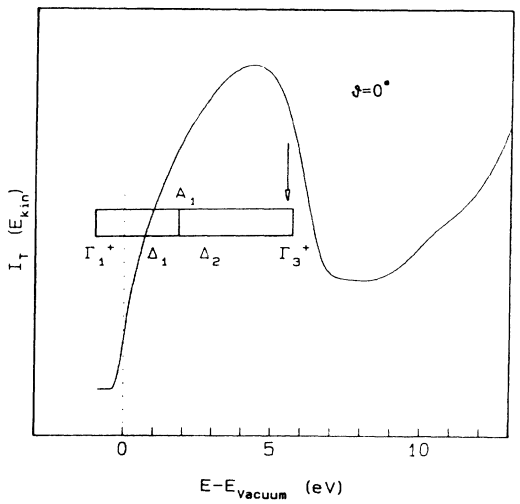

FIG. 5. The absorbed current just above the vacuum level. The inset shows the calculated energies and bandwidth of the interlayer state according to Holzwarth *et al.* (Ref. 1) with Hedin-Lundqvist exchange correlation. The arrow marks the maximum of the negative second derivative of the spectrum.

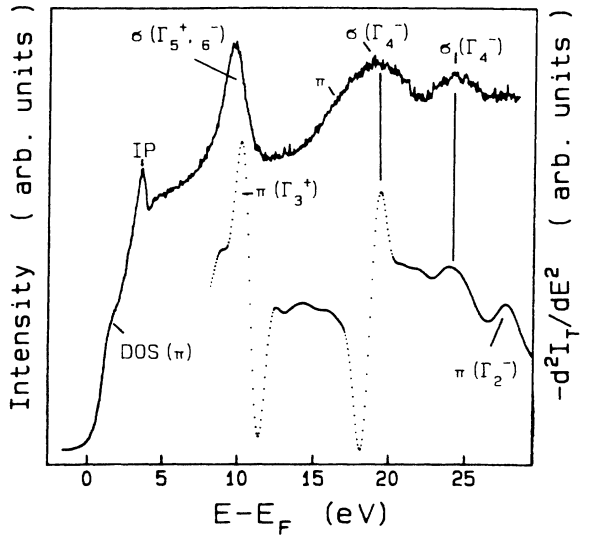

FIG. 6. Comparison of a normal incidence inverse photoemission spectrum (upper curve, background subtracted) with the negative second derivative of the target current spectrum (lower curve).

the normal incidence spectrum, since it reveals information about the dispersion of the bands parallel to the c axis in ΓA direction. The spectrum in Fig. 5 taken for normal incidence was measured with a slightly negative biased sample ($\sim$4.5 V) to study the region in the vicinity of the vacuum level and to measure the work function of graphite (4.7 eV) by the onset of the TCS spectrum. The range of the first current maximum in the undifferentiated spectra at $\vartheta = 0°$ (Figs. 4 and 5) extends from the vacuum level up to about 6 eV $E_{\rm kin}$. This region of enhanced electron takeup is clearly attributable to the interlayer state, which is connected by a strong $k_\perp$ dispersion with the antibonding (Γ_3^+) band. The inset in Fig. 5 shows the calculated[1] range of the $k_\perp$ dispersion which is in good agreement with the TCS measurements. Part of its $k_\perp$ dispersion has been measured with ARIPS using variable photon energy.[17] Due to the large value for the real part of optical potential of graphite it was not possible to map the whole range of the dispersion in that experiment. Therefore a complete comparison with TCS is not possible. We assume that the bottom of this interesting interlayer state (Γ_1^+) lies between the image potential state at 3.7 eV and the vacuum level (4.7 eV). The top, i.e., the $\pi(\Gamma_3^+)$ state, is located near the maximum of the negative second derivative (Fig. 5) at 5.5 eV $E_{\rm kin}$ which is often slightly shifted from the band edge towards the center of the band.[27] Except for the ARIPS measurements of Fauster *et al.*[17] and another recent ARIPS experiment,[19] the interlayer state has not been observed experimentally so far by other spectroscopies because of its low DOS, its *s*-like character and the small overlap with occupied states.[6] Due to the different process involved TCS yields a pronounced maximum. It is important to state here that the *emission E* in the ARIPS spectra at 9.7 eV (Figs. 1 and 3), if interpreted as ($\Gamma_5^+, 6^-$) as discussed above, is not responsible for the TCS emission in this region because at nor-

mal incidence only Bloch waves with Δ_1 or Δ_2 symmetry (and not with Δ_5,Δ_6 symmetry) couple to the incident beam.[13]

The broad maximum around 15 eV above the vacuum level (Fig. 4) is attributable to an also strongly $k_\perp$ dispersing σ band with Γ_4^- symmetry at its bottom.[2] The corresponding maximum in the negative second derivative is at 19.5 eV above E_F. The calculated value[2] is a little higher (21.7 eV). This state at 19.5 eV and a still higher-lying state at 24 eV above E_F have been observed with both ARIPS and TCS as shown in Fig. 6. The figure gives a comparison of an ARIPS spectrum over a large energy range at normal incidence and the negative second derivative of a TCS spectrum measured under exactly the same conditions, i.e., identical sample surface and range of acceleration voltage of the electron source. The abscissa of the experimental TCS spectrum is simply shifted by the photon energy of the band-pass detector in order to define the common energy scale for both spectra. The characterization of the measured states above the $\sigma(\Gamma_4^-)$ state at 19.5 eV is somewhat difficult. The state at about 24 eV above E_F (ARIPS, TCS in Fig. 6) cannot be attributed to the $\sigma(\Gamma_1^+)$ state lying just above $\sigma(\Gamma_4^-)$ in the calculation[2] (see Fig. 8). Both states are connected by a Δ_2-Δ_1-$k_\perp$ dispersion and should not be observable together in an ARIPS spectrum.[13] So we may attribute the emission at about 24 eV (ARIPS, TCS) to the still higher-lying $\sigma(\Gamma_4^-)$ state in Ref. 2.

Another interesting feature in Fig. 4 is the structure strongly downward dispersing with increasing angle clearly visible at high angles of incidence ($\vartheta=70°$, $E_{\text{kin}}=9.5$ eV). We assume the top of this band at normal incidence at 23 eV E_{kin}. Its dispersion and binding energy is in rather good agreement with the strongly dispersing $\pi(\Gamma_2^-,K_6,M_3^+)$ band of the calculation.[2] But it cannot be excluded with certainty that the top at 23 eV E_{kin} belongs to a π band above this $\pi(\Gamma_2^-)$ whose energy maximum is out of the range of the calculation of Tatar and Rabii.[2] If this is correct the $\pi(\Gamma_2^-)$ state probably coincides in energy at Γ with the $\sigma(\Gamma_4^-)$ state[2] (about 24 eV above E_F in ARIPS and TCS, Fig. 6). Up to 30° the experimentally derived dispersion of the π state (23 eV E_{kin} at $\vartheta=0°$) is disturbed by crossing σ states. The lower part of this π state and the σ state at about 19.5 eV above E_F ($k_{||}=0$) are in good agreement with ARSEES data using synchrotron radiation.[16]

In the TCS spectrum at $k_{||}=0$ only those states of Δ_1,Δ_2 symmetry are visible which have a large $k_\perp$ dispersion. With increasing angle of incidence also bands with small $k_\perp$, but larger $k_{||}$ dispersion like the π band (with its top Γ_2^- at 23 eV E_{kin}, $k_{||}=0$), gain intensity. This leads to the view that only those Bloch states transport sample current effectively whose group velocity has a considerable component in the direction of the velocity of the incoming plane wave entering the sample (see also Ref. 16).

C. Comparison with band-structure calculations

Figures 7 and 8 give the final comparison of the band structure from the combined ARIPS and TCS data with

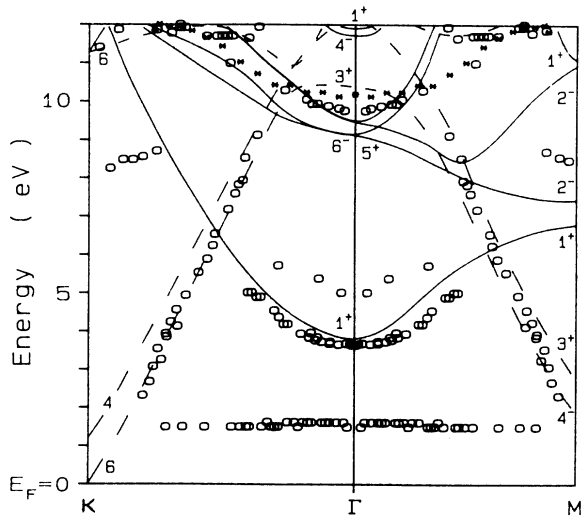

FIG. 7. Comparison of the experimental band structure (○,*) with the calculation of Holzwarth *et al.* (Ref. 1) using Hedin-Lundqvist exchange correlation, π bands (dashed lines), σ bands (solid lines). The same experimental data are plotted in the ΓM and ΓK direction: inverse photoemission (○), maxima of the negative second derivative of the target current spectrum (*).

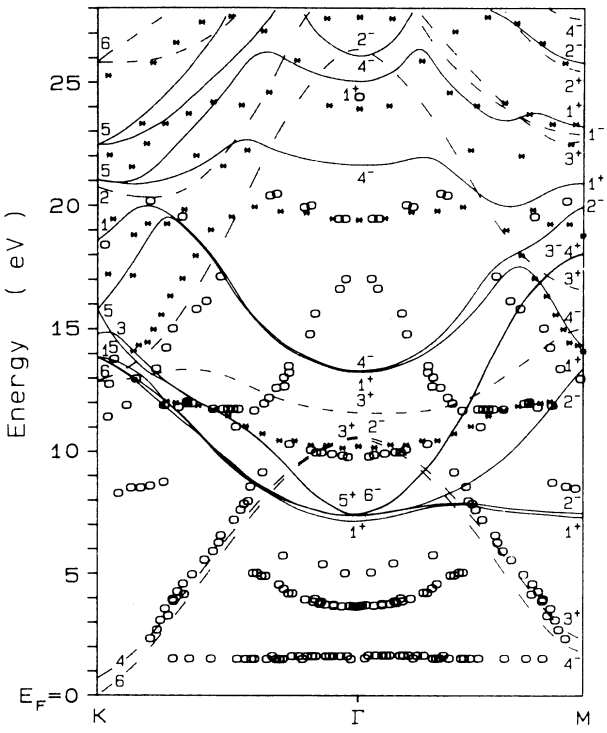

FIG. 8. Experimental data (○,*) as in Fig. 7, but extended to higher energies, now compared with the calculation of Tatar and Rabii (Ref. 2), π bands (dashed lines), σ bands (solid lines).

the calculations of Holzwarth *et al.*[1] using the Hedin-Lundqvist exchange correlation (Fig. 7) and Tatar and Rabii[2] (Fig. 8). The experimental band structure of the azimuthal disordered graphite obtained by applying the usual $k_{||}$ analysis to the ARIPS data and the maxima of the negative second derivative of the TCS spectra is compared with both directions of high symmetry ($\Gamma M, \Gamma K$). In the energy range of the calculation of Holzwarth *et al.*[1] the agreement is convincing. Especially the energy and dispersion of the lowest π band is exactly reproduced within the experimental error. Also the energies of the σ state at about 9.7 eV and its $k_{||}$ dispersion is in quite good agreement with Ref. 1. Despite some major discrepancies in the low-energy range concerning the σ bands the calculation of Tatar and Rabii gives good results with regard to the shape of the dispersion of the bands. Considering the difficulty to calculate the correct energies in the range of this calculation theoretical and measured energies agree reasonably well. For example, for the top of the high-lying π band (Γ_2^-) TCS gives 27.7 eV, the calculation 26.4 eV. The energies of the σ states at Γ are 19.5 eV (Γ_4^-) and 24 eV (Γ_4^-) (TCS and ARIPS) and the calculation yields 21.7 and 25.2 eV, respectively.

The only band not reproduced in the calculations is the strongly dispersing state with the top (Γ) at 17 eV which we assign a π character. In comparing both calculations[1,2] that of Holzwarth *et al.*[1] gives a far better agreement with the experimental data. As mentioned by Holzwarth *et al.* the reason for the pronounced differences in energy and dispersion in the two calculations is the self-consistency in their calculation which increases the charge density outside the bonding region. This causes a stronger attractive potential in the interlayer region. Thus, for example, the interlayer state $\sigma(\Gamma_1^+)$ is lowered in energy yielding a very different behavior of the lowest σ manifold at Γ as compared to Tatar and Rabii.[2]

IV. CONCLUSION

We have studied the energy and dispersion of π- and σ-conduction states of graphite (HOPG) over a large energy range up to about 35 eV above the Fermi level by combining angular-resolved photoemission and target current spectroscopy. A surface state just below the vacuum level is attributed to the $n=1$ image potential state. The comparison with band calculations gives the best agreement with that of Holzwarth *et al.* using the Hedin-Lundqvist exchange correlation. Target current spectroscopy turned out to be an effective method for the investigation of $k_\perp$ bandwidths and $k_{||}$ dispersions of unoccupied states above the vacuum level providing relevant data in an easier way than angle-resolved secondary electron spectroscopy. Due to the different processes involved target current spectroscopy yields extra information supplemental to inverse photoemission. Both spectroscopies complement each other well. The results presented on graphite in this paper, in particular the combination of both spectroscopies, are expected to stimulate further experimental and theoretical work on the conduction states of also other materials including higher energies well above the vacuum level.

ACKNOWLEDGMENTS

We thank A. Marx (IBM) for providing the HOPG sample, R. L. Johnson (MPI Stuttgart) for technical support, and E. Pehlke and W. Schattke (Universität Kiel) for discussions on theoretical aspects. This work was supported in part by the Deutsche Forschungsgemeinschaft.

[1]N. A. W. Holzwarth, S. G. Louie, and S. Rabii, Phys. Rev. B **26**, 5382 (1982).
[2]R. C. Tatar and S. Rabii, Phys. Rev. B **25**, 4126 (1982).
[3]C. P. Mallet, J. Phys. C **14**, L213 (1981).
[4]A. Zunger, Phys. Rev. B **17**, 626 (1978).
[5]R. F. Willis, B. Fitton, and G. S. Painter, Phys. Rev. B **9**, 1926 (1974).
[6]M. Posternak, A. Baldereschi, A. J. Freeman, E. Wimmer, and M. Weinert, Phys. Rev. Lett. **50**, 761 (1983).
[7]M. Posternak, A. Baldereschi, A. J. Freeman, and E. Wimmer, Phys. Rev. Lett. **52**, 863 (1984).
[8]D. M. Williams, Nuovo Cimento **38b**, 216 (1977).
[9]W. Eberhardt, I. T. McGovern, E. W. Plummer, and J. E. Fisher, Phys. Rev. Lett. **21**, 200 (1980).
[10]A. R. Law, J. J. Barry, and H. P. Hughes, Phys. Rev. B **28**, 5332 (1983).
[11]D. Marchand, C. Fretigny, M. Lagües, F. Battalan, Ch. Simon, I. Rosenmann, and R. Pinchaux, Phys. Rev. B **30**, 4788 (1984).
[12]A. R. Law, M. T. Johnson, and H. P. Hughes, Phys. Rev. B **34**, 4289 (1986).
[13]D. Pescia, A. R. Law, M. T. Johnson, and H. P. Hughes, Solid State Commun. **56**, 809 (1985).
[14]T. Takahashi, H. Tokailin, and T. Sagawa, Solid State Commun. **52**, 765 (1984).
[15]T. Takahashi, H. Tokailin, and T. Sagawa, Phys. Rev. B **32**, 8317 (1985).
[16]M. T. Johnson, A. R. Law, and H. P. Hughes, Surf. Sci. **162**, 11 (1985).
[17]Th. Fauster, F. J. Himpsel, J. E. Fisher, and E. W. Plummer, Phys. Rev. Lett. **51**, 430 (1983).
[18]I. Schäfer, M. Schlüter, and M. Skibowski, Proceedings of the Eighth International Conference on Vacuum UV Radiation Physics, Extended Abstract, Lund, 1986, edited by P. O. Nilsson (unpublished), p. 529.
[19]I. R. Collins, and P. T. Andrews, Proceedings of the Eighth International Conference on Vacuum UV Radiation Physics, Extended Abstract, Lund, 1986, edited by P. O. Nilsson (unpublished), p. 533.
[20]B. Reihl, J. K. Gimzewski, J. M. Nicholls, and E. Tosatti, Phys. Rev. B **33**, 5770 (1986).
[21]D. Straub and F. J. Himpsel, Phys. Rev. B **33**, 2256 (1986).
[22]V. Dose, Prog. Surf. Sci. **13**, 225 (1983).
[23]N. V. Smith, Vacuum **33**, 803 (1983).
[24]J. B. Pendry, J. Phys. C **14**, 1381 (1981).
[25]E. G. McRae, J. M. Landwehr, and C. W. Caldwell, Phys. Rev. Lett. **38**, 1422 (1977).
[26]R. C. Jaklevic and L. C. Davis, Phys. Rev. B **26**, 5391 (1982).
[27]E. Tamura, R. Feder, and J. Krewer, Solid State Commun. **55**, 543 (1985).

[28]L. T. Chadderton and S. A. Komolov, Surf. Sci. **90**, 359 (1979).
[29]A. Dittmar-Wituski, M. Naparty, and J. Skonieczny, J. Phys. C **18**, 2563 (1985).
[30]N. Babbe, W. Drube, I. Schäfer, and M. Skibowski, J. Phys. E **18**, 158 (1985).
[31]I. Schäfer, W. Drube, M. Schlüter, G. Plagemann, and M. Skibowski, Rev. Sci. Instrum. (to be published).
[32]R. Klucker, M. Skibowski, and W. Steinmann, Phys. Status Solidi **65**, 703 (1974), and references therein.
[33]Strong contamination was obtained accidentally by a failure in the lense voltages of the electron gun resulting in electron-induced desorption from the lense surfaces. The emission *C* was the only state affected thereby and almost vanished.
[34]Y. Baer, J. Electron Spectrosc. Relat. Phenom. **24**, 95 (1981).
[35]V. Dose, G. Reusing, and H. Scheidt, Phys. Rev. B **26**, 984 (1982).
[36]J. F. Morar, F. J. Himpsel, G. Hollinger, J. L. Jordan, G. Hughes, and F. R. McFeely, Phys. Rev. B **33**, 1346 (1986).